PCCP

PAPER

View Article Online
View Journal | View Issue

Cite this: *Phys. Chem. Chem. Phys.*, 2023, **25**, 28437

Exciton delocalization in a fully synthetic DNA-templated bacteriochlorin dimer†

Olga A. Mass, *[a] Devan R. Watt, [a] Lance K. Patten, [a] Ryan D. Pensack, [a] Jeunghoon Lee, [ac] Daniel B. Turner, [a] Bernard Yurke[ab] and William B. Knowlton[ab]

A bacteriochlorophyll *a* (**Bchla**) dimer is a basic functional unit in the LH1 and LH2 photosynthetic pigment–protein antenna complexes of purple bacteria, where an ordered, close arrangement of **Bchla** pigments—secured by noncovalent bonding to a protein template—enables exciton delocalization at room temperature. Stable and tunable synthetic analogs of this key photosynthetic subunit could lead to facile engineering of exciton-based systems such as in artificial photosynthesis, organic optoelectronics, and molecular quantum computing. Here, using a combination of synthesis and theory, we demonstrate that exciton delocalization can be achieved in a dimer of a synthetic bacteriochlorin (**BC**) featuring stability, high structural modularity, and spectral properties advantageous for exciton-based devices. The **BC** dimer was covalently templated by DNA, a stable and highly programmable scaffold. To achieve exciton delocalization in the absence of pigment–protein interactions critical for the **Bchla** dimer, we relied on the strong transition dipole moment in **BC** enabled by two auxochromes along the Q_y transition, and omitting the central metal and isocyclic ring. The spectral properties of the synthetic "free" **BC** closely resembled those of **Bchla** in an organic solvent. Applying spectroscopic modeling, the exciton delocalization in the DNA-templated **BC** dimer was evaluated by extracting the excitonic hopping parameter, J to be 214 cm^{-1} (26.6 meV). For comparison, the same method applied to the natural protein-templated **Bchla** dimer yielded J of 286 cm^{-1} (35.5 meV). The smaller value of J in the **BC** dimer likely arose from the partial bacteriochlorin intercalation and the difference in medium effect between DNA and protein.

Received 10th April 2023,
Accepted 23rd August 2023

DOI: 10.1039/d3cp01634j

rsc.li/pccp

Introduction

A dimer of photosynthetic pigment bacteriochlorophyll *a* (**Bchl*a***) is the basic functional unit of the light-harvesting antenna system in purple bacteria.[1,2] Namely, 16 dimers of **Bchl*a*** form a B875 ring in the core antenna LH1, and 8–9 dimers form a B850 ring in the peripheral antenna LH2. The close positioning of the pigments in the **Bchl*a*** dimer with a center-to-center distance of about 9 Å results in the collective sharing of the excited states.[2] In such collective sharing, the excited state of a dimer (a molecular exciton or Frenkel exciton[3]) can be viewed as a quasiparticle that resides on one neighboring pigment or another according to the quantum-mechanical principle of superposition. In other words, the exciton is delocalized between the two pigments. The exciton delocalization extended to other dimers in each antenna ring enables excitation energy transfer to the reaction center with a high quantum efficiency.[2,4–6] The quantum state of exciton delocalization that a photosynthetic antenna maintains at ambient temperatures and in often harsh environmental conditions is highly desirable for engineering excitonic systems[7–9] in artificial photosynthesis,[10,11] organic optoelectronics,[12–14] and room temperature quantum computing.[15–18] Hence, it is important to access stable and tunable synthetic analogs of **Bchl*a*** dimer exhibiting exciton delocalization at room temperature.

The structural basis of **Bchl*a*** is a tetrahydroporphyrin, a $4e^-/4H^+$ reduced porphyrin with alternating pyrrole and pyrroline rings known as bacteriochlorin macrocycle. The steady-state absorption spectrum of the bacteriochlorin chromophore consists of four characteristic porphyrin bands: the fundamental Soret bands B_y and B_x, and the Q_x and Q_y bands.

[a] *Micron School of Materials Science & Engineering, Boise State University, Boise, Idaho 83725, USA. E-mail: olgamass@boisestate.edu*
[b] *Department of Electrical & Computer Engineering, Boise State University, Boise, Idaho 83725, USA*
[c] *Department of Chemistry and Biochemistry, Boise State University, Boise, Idaho 83725, USA*

† Electronic supplementary information (ESI) available: ^1H NMR and ^{13}C NMR spectra, oligo sequences, ESI-MS and electrophoresis of dye-labeled strands, absorption spectra of bacteriochlorin **2** and **3**, 230–850 nm absorption spectra of DNA-bacteriochlorin constructs, fluorescence data, and KRM modeling. See DOI: https://doi.org/10.1039/d3cp01634j

In bacteriochlorin, the Q_y band responsible for the light absorption to produce the lowest singlet excited state is significantly more intense ($\varepsilon \sim 100\,000\ cm^{-1}\ M^{-1}$) and redshifted than that in the porphyrin due to the reduction of the porphyrin opposing pyrrole rings. Such long-wavelength absorption can enable pure exciton states not mixed with the transitions of the UV region, which—in addition to the exceptional narrowness and minimal vibronic structure of the bacteriochlorin Q_y band—are spectral features strongly advantageous for engineering exciton circuits.[15]

According to the molecular exciton model developed by Kasha,[3] exciton delocalization is primarily enabled by the excitonic Coulombic coupling of the dye transition dipole moments (TDMs). The intermolecular chromophore distance strongly influences the strength of the excitonic coupling. An intermolecular distance that is too short can result in concentration quenching.[19] In contrast, a distance that is too long prevents excitonic coupling; transfer of the excitation energy then occurs *via* the Föster mechanism between an acceptor and donor chromophore, as seen between the antenna rings B800 to B850 or B850 to B875.[5] In the photosynthetic antenna of purple bacteria, the ideal intermolecular distance of 0.4–1.0 nm and orientation of **Bchl*a*** is maintained by a protein scaffold. In both LH1 and LH2, a **Bchl*a*** dimer is templated by an α/β apoprotein subunit; though, the protein subunit of LH2 contains an additional distant **Bchl*a*** monomer.[2] In addition to securing relative positions of **Bchl*a*** dyes, specific non-covalent interactions between amino acids and **Bchl*a*** are thought to enhance its TDM, and red-shift its site energy.[20,21]

The examples of bacteriochlorin dimer exhibiting signatures of excitonic coupling and delocalization are limited to a few reported systems created for fundamental studies of photosynthesis and utilizing natural **Bchl*a*** or its semisynthetic derivatives. Namely, in the absence of a scaffold, a dimer of isolated **Bchl*a*** was formed *via* self-aggregation in solution,[22,23] and by tethering **Bchl*a*** dyes *via* a non-conjugating linker.[24] In addition, a **Bchl*a*** dimer was non-covalently templated by natural α/β apoprotein (reconstructed **820B** complex),[25] and by synthetic proteins.[26,27] The limitation of the self-aggregation method is the presence of a large monomer population or high-order aggregates; while linking two dyes or utilizing non-covalent protein templating is limited to small size aggregates of 1–2 dyes. Using proteins as scaffolds can also be challenging due to their strong propensity to aggregate in solution, conformational sensitivity to modifications, and complex design rules based on 24 amino acid building blocks. Another challenge associated with the above systems is the instability of natural and semisynthetic **Bchl*a*** due to its favorable conversion into a porphyrin and limited synthetic tunability owing to a full set of substituents around the **Bchl*a*** macrocycle. These studies highlighted the need for (1) stable and tunable bacteriochlorin, and (2) a covalent templating method with a stable scaffold that can yield precise control over the number of dyes in small and high-order dye aggregates.

DNA is a versatile scaffold owing to its predictable and robust self-assembly and stability,[28,29] and simple design rules of only 4 nucleotides encoding the structure of the DNA. Having a hydrophilic negatively charged backbone, DNA is stable in an aqueous solution. The structure of the DNA is robust to local modifications. Further, a dye can be tethered to a specific site of DNA *via* a variety of covalent linkers, thus enabling control over the number of dyes and their positions relative to the DNA.[30] These advantages of dye covalent templating *via* DNA enabled exciton delocalization in aggregates of such dye families as azo dyes,[31–33] merocyanines,[34] polymethine dyes,[35–43] squaraines,[44–48] and perylenes.[49] While several studies have shown that aggregates of porphyrins,[50–54] the most related dye family to bacteriochlorins, can be covalently templated *via* DNA, the extent of exciton delocalization was not assessed.

Here, we explored if a fully synthetic DNA-templated bacteriochlorin dimer can exhibit exciton delocalization. We employed a specific type of branched DNA structure, a 4-arm DNA construct known as a Holliday Junction (HJ) that was previously shown to template a variety of dyes *via* a post-modification of the HJ core[36,43,47] and was shown to be particularly advantageous in solubilizing hydrophobic molecules.[47] For the dye, we synthesized a novel analog of **Bchl*a*** using a *de novo* bacteriochlorin methodology developed by Lindsey.[55,56] Bacteriochlorins available through this methodology are designed with geminal dimethyl groups in pyrroline rings to make them far more chemically and thermally stable than natural **Bchl*a***. The diversity of *de novo* bacteriochlorin synthetic modifications enabled us to create bacteriochlorin (**BC**) with a large TDM comparable with that of **Bchl*a***, as well as equip **BC** with a covalent linker for DNA tethering (Fig. 1). To assess the suitability of DNA to template a bacteriochlorin dimer exhibiting exciton delocalization, we calculated the strength of the excitonic coupling in terms of the excitonic hopping parameter, *J*, in the DNA-templated bacteriochlorin dimer and the natural **Bchl*a*** dimer templated by α/β apoprotein in solution known as **820B** complex. Semiempirical modeling of steady-state spectra based on the theoretical approach of Kühn, Renger, and May[57] determined *J* values of 26.6 and 35.5 meV in bacteriochlorin and **Bchl*a*** dimers, respectively, as well as their distinct dimer geometries. While **BC** exhibited TDM sufficiently high to achieve exciton delocalization in the aqueous DNA environment and the absence of dye–protein interactions, bacteriochlorin dimerization was likely disrupted by partial intercalation into DNA. Collectively, these results indicate that DNA nanotechnology can be a facile means to achieve exciton delocalization in synthetic bacteriochlorin aggregates by selecting complementary bacteriochlorin chemical structures and DNA templates.

Results

Dye design

To create a DNA-templated dimer for this study, we chose the synthetic bacteriochlorin analog of natural **Bchl*a*** depicted in Fig. 1 as **BC**. The synthetic **BC** contains a bacteriochlorin macrocycle of **Bchl*a*** but exhibits greater thermal and chemical stability due to the presence of geminal dimethyl groups that

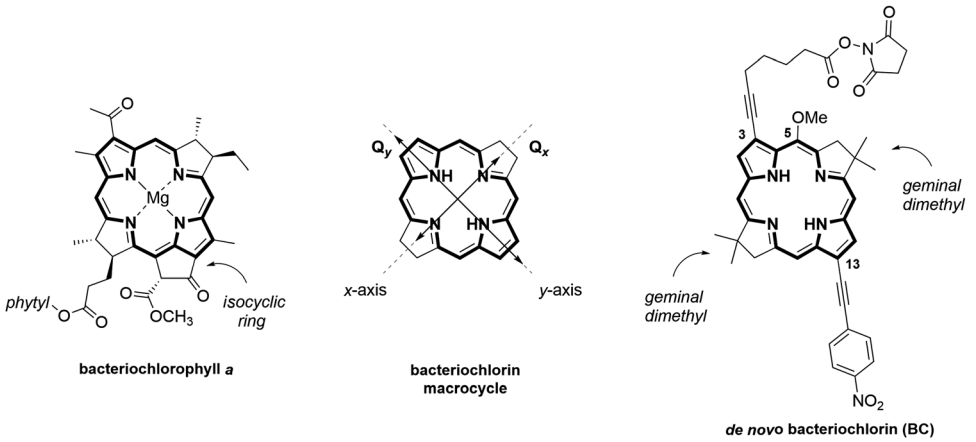

Fig. 1 Chemical structures of (left) natural bacteriochlorophyll *a*, (center) bacteriochlorin macrocycle depicting Q_x and Q_y transitions polarized along molecular *x*- and *y*-axis, respectively, and (right) synthetic bacteriochlorin **BC**.

prevent dehydrogenation into a porphyrin. Established *de novo* methodology for synthetic bacteriochlorins offers diverse synthetic modularity of their chemical and photophysical properties.[55,58,59] The **BC** side substituents were selected to increase the Q_y transition dipole moment magnitude, which is critical for stronger excitonic coupling.[60] Survey studies demonstrated that auxochromes—functional groups that alter the spectral properties of a chromophore—positioned along the Q_y TDM axis (attachment sites 2-, 3- and 12-, 13-) have the strongest influence on bacteriochlorin spectral properties. Specifically, ethynyl-type groups caused a significant enhancement of Q_y magnitude.[61] Based on these observations, we designed **BC** to carry 13-(4-nitrophenyl)ethynyl and 3-ethynyl auxochromes and *N*-hydroxysuccinimide ester (NHS) linker for DNA tethering. The presence of the isocyclic ring and the central metal were shown to cause Q_y to redshift, but had a small effect on Q_y magnitude,[62] and were therefore omitted in the **BC** structural design. The methoxy group at the 5-position was installed to provide the means for the asymmetric chemical derivatization of the macrocycle.[63]

Chemical synthesis

The synthesis of the target NHS-bacteriochlorin **BC** for tethering to DNA relied on the selective derivatization of the 3,13-dibromo-5-methoxybacteriochlorin building block (Fig. 2). First, β-bromodihydrodipyrrin-acetal **1** was prepared according to the established streamlined multistep synthesis.[64] Self-condensation of **1** into **2** in the presence of TMSOTf/2,6-DTBP was carried out according to the reported procedure[55] with several modifications. In particular, reducing the amount of TMSOTf from 5 to 3 molar equivalents, added in increments over 1 h, afforded **2** with 92% purity in 54% yield. Monitoring the reaction progress by thin layer chromatography indicated reaction completion in 3 h. We found that high purity of **1** is critical for achieving a high yield of its self-condensation. Next, bacteriochlorin **2** was subjected to two subsequent Sonogashira reactions under the conditions for asymmetric disubstitution previously developed by Yu and Ptaszek, taking advantage of the 5-methoxy group sterically hindering the 3-position.[63] Compound **2** was treated with 1-ethynyl-4-nitrobenzene in the presence of $Pd(PPh_3)_4$ and K_2CO_3 in DMF to afford **3** functionalized with 13-(4-nitrophenyl)ethynyl group in 28% yield; small amounts of the disubstituted product and unreacted starting material were observed. Treatment of **3** with 6-heptynoic acid NHS ester **4**, catalyzed by $(PPh_3)_2PdCl_2$ in Et_3N/DMF, afforded the desired NHS ester **BC** in 18% yield. Newly reported compounds **3** and **BC** were characterized by ^1H NMR, ^{13}C NMR, ESI-MS, steady-state absorption, and fluorescence spectroscopies.

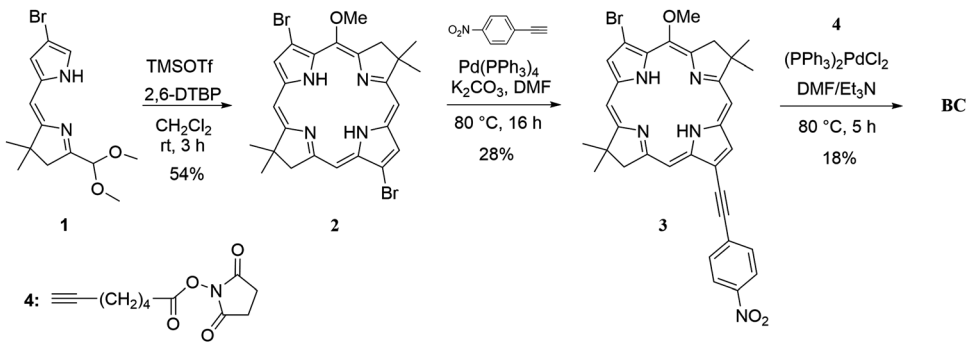

Fig. 2 Synthetic route to the *de novo* NHS ester bacteriochlorin **BC**.

DNA templating

To template a **BC** dimer covalently to DNA, we chose a four-armed HJ construct. Previously, we showed that conformational isomerization of HJ between two isoforms[65] could result in a racemic mixture of two dimer enantiomorphs tethered to DNA *via* covalent linkers of equal length.[66] In that study, we also employed covalent linkers of unequal length to cause a conformational bias toward one HJ isoform and, hence, one optical isomer of the dimer.[66] Here, we implemented an alternative approach to avoid HJ conformational isomerization by spanning two HJ arms *via* a short chain of 14 unpaired thymidines. This approach was employed previously to constrain an unlabeled HJ.[67,68] The HJ was assembled using three oligo strands: A, C, and BD containing the thymidine chain. Oligo strands C and BD were internally modified with the amino thymidine T* for dye tethering. The **BC** in the form of NHS esters were tethered to BD and C oligo strands (Fig. 3a), purified by high-performance liquid chromatography, and characterized by ESI-MS at Integrated DNA Technologies (Section S2, ESI†). To create HJ constructs, oligo strands A, C, and BD were combined in equimolar amounts in aqueous buffer 1× TBE 15 mM $MgCl_2$ to the final concentration of 1.5 μM or 4.0 μM. Due to the sensitivity of bacteriochlorins to high temperatures, we avoided a standard DNA anneal procedure, which would have required heating the samples to 94 °C followed by cooling. Instead, to hybridize oligos into HJs, the samples were incubated at room temperature for 2 h. In this manner, we created the **BC** dimer and a control monomer construct (Fig. 3b). The formation of **BC**–HJ constructs was confirmed by non-denaturing polyacrylamide gel electrophoresis (Section S3, ESI†).

Optical properties

Spectral properties of "free" **BC** (*i.e.*, not covalently attached to DNA) were characterized by measuring absorption and fluorescence in toluene at room temperature. Free **BC** exhibited an absorption spectrum characteristic for bacteriochlorins featuring four absorption bands: $B_y(0,0)$ Soret at 355 nm, $B_x(0,0)$ Soret at 375 nm, $Q_x(0,0)$ at 530 nm, and Q_y (0,0) at 757 nm (Fig. 4 and Table 1). For comparison, the synthetic precursors 3,13-dibromo bacteriochlorin **2** without ethynyl groups and bacteriochlorin **3**, containing one ethynyl group at the 13-position, absorbed at 723 and 749 nm, respectively (Fig. S10, ESI†). The serial redshift of the Q_y band upon ethynyl mono and disubstitution indicated that both ethynyl groups were strongly conjugated with the macrocycle in **BC**. A weak vibronic progression was observed to higher energy in the absorption spectrum of **BC**. As typical for synthetic bacteriochlorins, the Q_y band was exceptionally narrow with a full width at half-maximum (fwhm) of 23 nm (402 cm^{-1}). To evaluate the molar extinction of the long-wavelength absorption band in **BC**, we relied on the established approach[61] to calculate the peak-intensity ratio and integrated manifold ratio of Q_y and Soret (B_y and B_x), then compared the ratios to those of **Bchl*a*** (Table 1). The absorption manifolds of **BC** and **Bchl*a*** were similar, indicating that the molar extinction of Q_y in **BC** should be at least as large as the reported extinction of **Bchl*a*** of 92 000 cm^{-1} M^{-1}.[69] In addition, we measured the absorption of "free" **BC** in a protic solvent such as ethanol for later comparison with the absorption of **BC** covalently attached to DNA in an aqueous environment (Fig. 4 and Table 1). From toluene to ethanol, **BC** exhibited a small blueshift and a small decrease in Q_y intensity relative to the Soret manifold. The observed effect of the protic solvent on

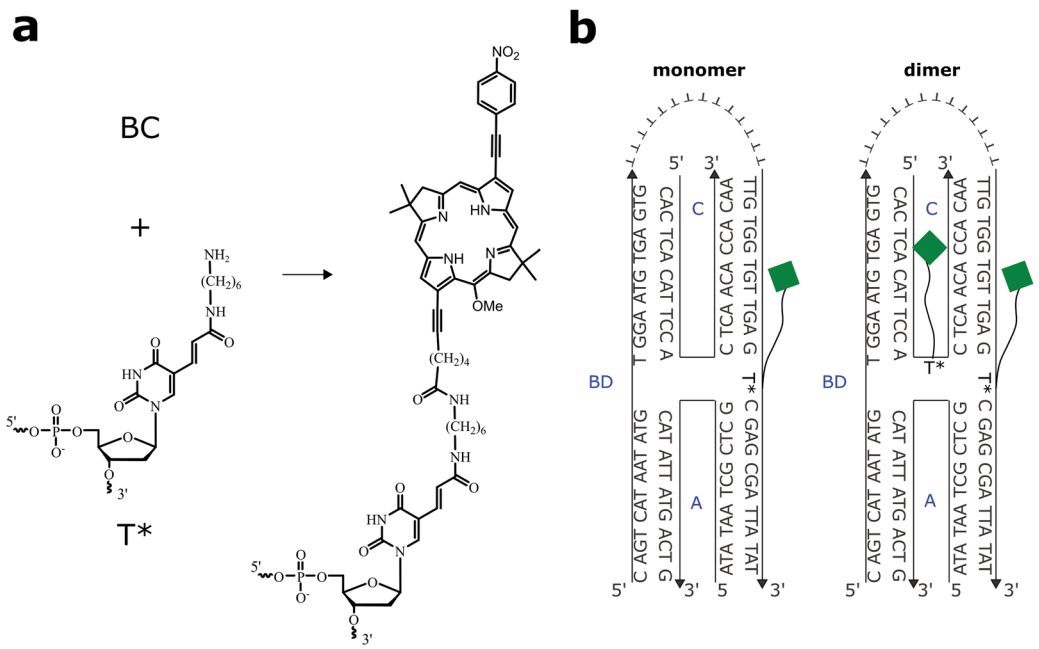

Fig. 3 Molecular designs of bacteriochlorin–DNA constructs. (a) an oligo post-modification with **BC** depicting chemical structures of the thymidine amino modifier (T*) and the resulting structure of **BC** tethered to the thymidine in an oligo strand. (b) Schematics of **BC** monomer and **BC** dimer. Each green diamond represents **BC**. The HJ strands are labeled A, BD, and C. Strand BD contains a chain of 14 unpaired thymidines.

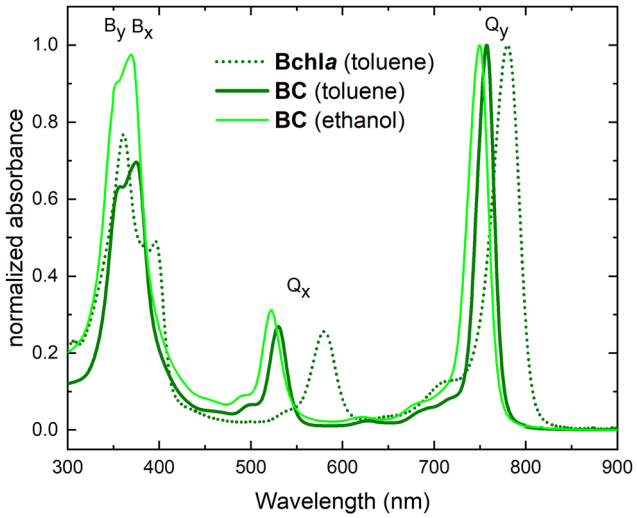

Fig. 4 Acquired steady-state absorption spectrum of "free" **BC** in toluene (solid dark green) and in ethanol (solid light green) and a reference spectrum of "free" **Bchl*a*** (dotted green) in toluene obtained from ref. 69. The spectra are normalized at the Q_y maximum.

BC absorption was in good agreement with a previous report on structurally similar synthetic bacteriohlorins.[70] Lastly, the **BC** fluorescence peaked at 761 nm in toluene (756 nm in ethanol), yielding a Stokes shift of 3 nm (4 nm in ethanol) (Fig. S11, ESI†). In ethanol, the **BC** fluorescence scaled by absorptance decreased by 20% compared to that in toluene.

The **BC** monomer covalently templated by HJ was characterized by steady-state absorption, fluorescence, and circular dichroism (CD) spectroscopies. To evaluate the solvating environment of the **BC** covalently attached to DNA, the spectral properties of the monomer (*i.e.*, a single dye attached to the strand BD in HJ) were compared to those of "free" **BC** in a nonpolar solvent such as toluene and in a polar protic solvent such as ethanol (Fig. 4 and 5a). The monomer exhibited the Soret maxima (B_y and B_x) at 356 and 375 nm, Q_x at 533 nm and Q_y at 767 nm. Relative to the "free" **BC** in toluene and ethanol, the monomer's Soret had minor redshifts with the reversed intensity ratio of B_y and B_x. In contrast, the Q bands exhibited more noticeable redshifts, with the Q_x red-shifted by 3 nm and 11 nm, and the Q_y red-shifted by 10 nm and 17 nm relative to toluene and ethanol, respectively. A significant redshift of the Q bands relative to the "free" **BC** in ethanol suggested the monomer being exposed to a nonpolar DNA groove solvation environment rather than an external aqueous environment. Another characteristic of the **BC**–DNA interaction was obtained from the spectral bandwidth. The Q_y bandwidth of the monomer [fwhm = 461 cm^{-1} (27 nm)] was comparable with that of "free" **BC** in ethanol and toluene, indicating that such events as macrocycle distortion or multiple modes of binding that would typically result in absorption broadening relative to the "free dye" did not take place in the **BC** monomer construct. Finally, the hypochromicity was evaluated by calculating monomer Q_y molar extinction. The DNA absorption peak appeared in the monomer spectrum at 260 nm (Fig. S12, ESI†). Based on the DNA theoretical extinction coefficient, the Q_y molar extinction (ε_{Q_y}) of the monomer was calculated to be 104 811 cm^{-1} M^{-1}. The value of ε_{Q_y} of the **BC** monomer is higher than that of free **Bchl*a*** in toluene,[69] which suggests no hyperchromicity effect in an aqueous DNA environment.

To gain more insight into the interactions of **BC** with DNA, we characterized the **BC** monomer by CD spectroscopy (Fig. 5b). The CD of the monomer exhibited a profound DNA bisignate couplet at 244 and 280 nm indicative of a well-formed B-DNA duplex. In the bacteriochlorin region, a weak negative feature (17 M^{-1} cm^{-1}) was observed in the vicinity of the Soret B_x region at 376 nm, while no signal was observed in the Q_x and Q_y regions. Since **BC** is achiral, the observed negative signal was attributed to the induced CD (ICD) due to the coupling between the DNA bases and a bacteriochlorin B_x Soret transition. The position of a ligand relative to DNA can be gauged from the sign and magnitude of the ICD.[71] A small positive ICD is typical for the intercalated ligands with the TDM oriented perpendicular to the base pair axis, while a small negative ICD occurs when the ligand TDM is parallel to the long base pair axis. On the other hand, a strong positive CD signal is associated with a ligand bound to the minor groove, thus having its TDM positioned 45° to the bases. Therefore, the small negative ICD in the vicinity of B_x suggested that bacteriochlorin could be oriented such that its *x*-molecular axis is parallel to the base pair long axis. Since bacteriochlorin molecular geometry is unfavorable for intercalation due to sterically bulky geminal dimethyl groups in the opposing pyrroline rings, the bacteriochlorin could be partially intercalated *via* its nitrophenyl substituent. This assumption was further supported by the reported strong intercalating propensity of nitrophenyl ligands.[72] The absence of the observed coupling between the Q_y transition and DNA was expected given the drastic difference in the Q_y and DNA transition energies. Lastly, the monomer did not exhibit fluorescence even at a high sample concentration of 4 μM (Fig. S11, ESI†). Only fluorescence traces from "free" **BC** were

Table 1 Absorption characteristics of "free" in solution synthetic **BC**[a] and natural **Bchl*a***[b]

"Free" dye	Solvent	λ B_y(0,0), B_x(0,0)/nm	λ Q_x(0,0)/nm	λ Q_y(0,0)/nm	ε Q_y/cm^{-1} M^{-1}	fwhm Q_y/cm^{-1} (nm)	I_{Q_y}/I_{B_y}[c]	I_{Q_y}/I_{B_x}[d]	$\sum_{Q_y}/\sum_B$[e]
BC	Ethanol	353, 369	522	750	—	466 (26)	1.12	1.03	0.64
BC	Toluene	355, 375	530	757	—	402 (23)	1.58	1.44	0.75
Bchl*a*	Toluene	361, 396	580	780	92 000	579 (35)	1.30	2.04	1.03

[a] At room temperature. [b] Absorption data from ref. 69 (in toluene). [c] Ratio of the intensities of the B_y(0,0) and Q_y(0,0) bands. [d] Ratio of the intensities of the B_x(0,0) and Q_y(0,0) bands. [e] Ratio of the integrated intensities of the B (B_y and B_x; 320–420 nm) and Q_y [Q_y(0,0) and vibrational progression including Q_y(1,0); 660–850 nm] bands.

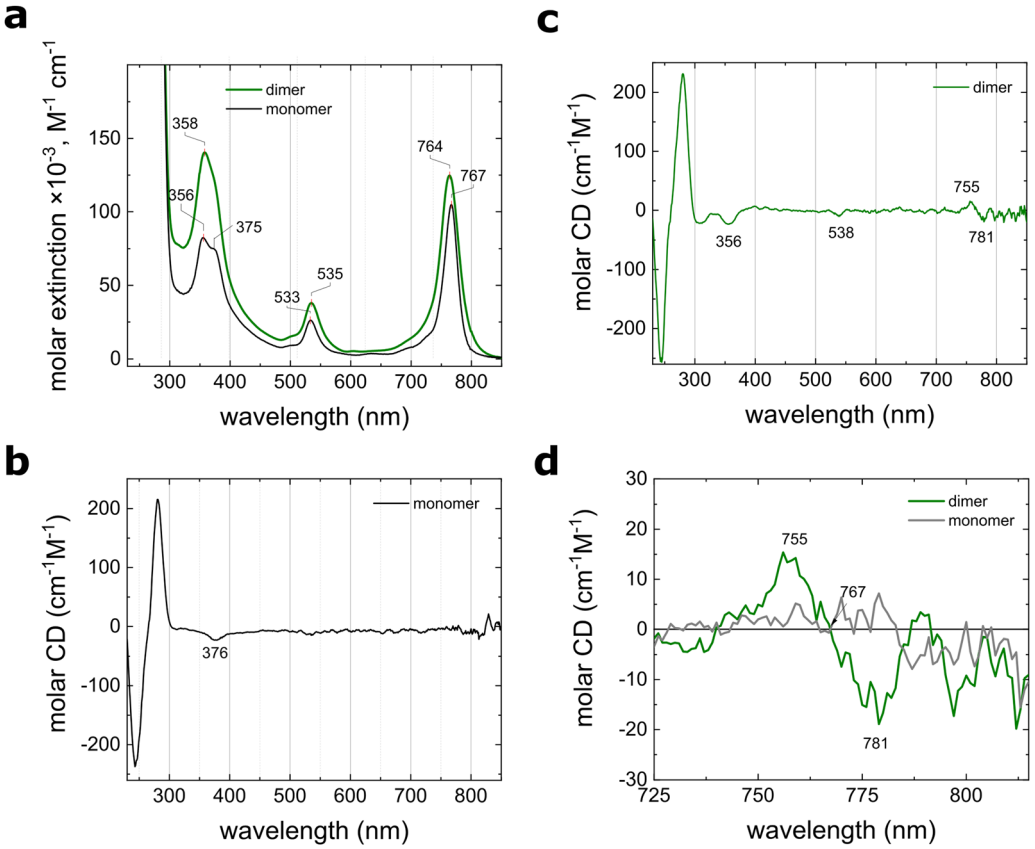

Fig. 5 (a) Acquired steady-state absorption of **BC** monomer and dimer tethered to HJ. The sample concentration for absorption was 1.5 μM in 1× TBE 15 mM $MgCl_2$. Acquired steady-state circular dichroism of (b) **BC** monomer, (c) **BC** dimer tethered to HJ, and (d) magnified Q_y region. The sample concentration for CD was 4.0 μM in 1× TBE 15 mM $MgCl_2$. The spectra were recorded at room temperature.

observed in the monomer sample. Fluorescence quenching of monomer could be explained with the partial bacteriochlorin intercalation or photoinduced electron transfer to DNA.[73,74]

Next, we performed steady-state spectroscopy to characterize the DNA-templated **BC** dimer. In the absorption spectrum, **BC** dimer exhibited the following changes relative to the monomer spectrum: Q_y blueshift from 767 nm to 764 nm, and Q_x and Soret redshifts of 2 nm (Fig. 5a and Fig. S12, ESI†). The perturbations in the dimer absorption relative to that of the monomer seemed to indicate a weak excitonic coupling between the chromophores in face-to-face or H-aggregate orientation. No fluorescence was observed in the **BC** dimer (Fig. S11, ESI†), indicating excited-state quenching often observed in H-aggregates.[75] An additional signature of excitonic coupling in the **BC** dimer was evident from its CD spectrum (Fig. 5c). The dimer exhibited three CD features in the dye region not observed in the CD spectrum of the monomer. First, the dimer showed a negative band at 356 nm corresponding to the B_y Soret absorption maximum. In addition, the dimer spectrum exhibited a negative band at 538 nm in the Q_x region, and a weak bisignate couplet with the intersection point at 767 nm corresponding to the monomer Q_y absorption maximum (Fig. 5d). The bisignate couplet was characterized by Cotton effects at 755 and 781 nm of equal magnitude and opposite sign indicative of the exciton-coupled dimer. Due to the small signal magnitude and its proximity to the noisy range of the 900 nm detector limit, we carried out several CD measurements optimizing the instrument settings; the Q_y bisignate couplet was consistently observed under different settings (Fig. S13, ESI†). While the dimer Soret and Q_x spectral features could arise from both **BC** excitonic coupling and electronic interactions with DNA bases, the spectral changes in the vicinity of Q_y were attributed solely to excitonic coupling and delocalization in the **BC** dimer. The Davydov splitting of 441 cm^{-1} (a difference between Cotton effects of the bisignate couplet) afforded spectral excitonic coupling strength of 220.5 cm^{-1} (27.4 meV).

Modeling

To quantify the strength of excitonic coupling responsible for exciton delocalization spectroscopically observed in the **BC** dimer, we applied semiempirical modeling[42,48] based on the theoretical approach of Kühn, Renger, and May (Section S8, ESI†).[57] For closely positioned and collectively excited chromophores, the excitonic coupling is primarily based on dipole–dipole Coulomb interaction of the TDMs. According to Kasha's molecular exciton model,[3] the strength of the Coulomb interaction (or hopping interaction) can be expressed with the exciton hopping parameter *J*. To determine *J* in the

bacteriochlorin dimer, we simultaneously modeled **BC** dimer experimental absorption and CD spectra utilizing a Holstein-like[76] Frenkel Hamiltonian[60] (eqn (S1), ESI†). In brief, the modeling generated various theoretical dimer configurations and calculated J as Coulomb dipole–dipole coupling for each dimer configuration using the extended dipole approximation[77] (eqn (S4), ESI†). Placing two point charges of the opposite sign along the Q_y transition accounted for the J dependence on the TDM center-to-center distance, angle, and displacement. The TDM magnitude of the DNA-templated **BC** monomer was determined from its experimental absorption spectrum to be 6.9 D (eqn (S5), ESI†). To account for the dye–DNA interactions and medium effect, the experimental TDM value of the monomer and solvent refractive index were incorporated in the numerical coefficient J_0 (eqn (S7), ESI†). Next, the J values were used to populate the Holstein-like augmented Frenkel Hamiltonian consisting of the electronic and vibronic components and generate theoretical absorption and CD spectra (eqn (S10) and (S11), ESI†). The theoretical spectra were compared with the experimental absorption and CD spectra and assigned a fitness score. The search for the best-fit spectra and the associated J value continued by iterations in TDM orientations guided by stochastic gradient descent. To ensure that the found dimer configuration was the unique solution to fit the experimental spectra, we modeled each system twice, starting with two extreme initial dimer configurations, face-to-face and end-to-end.

KRM modeling, as described above, was performed for two representative cases of the bacteriochlorin–HJ system. In Case 1, we assumed a homogeneous dimer system where bacteriochlorin dyes were fully available to form the dimer (Fig. 6a). In Case 2, we assumed a heterogeneous system of a dimer and two monomers, where a population of the intercalated dyes was not sterically available to form a dimer, thus resulting in excess of "optical" monomers (*i.e.*, distant dyes in the dimer HJ construct) and a dimer population (Fig. 6b). When modeling

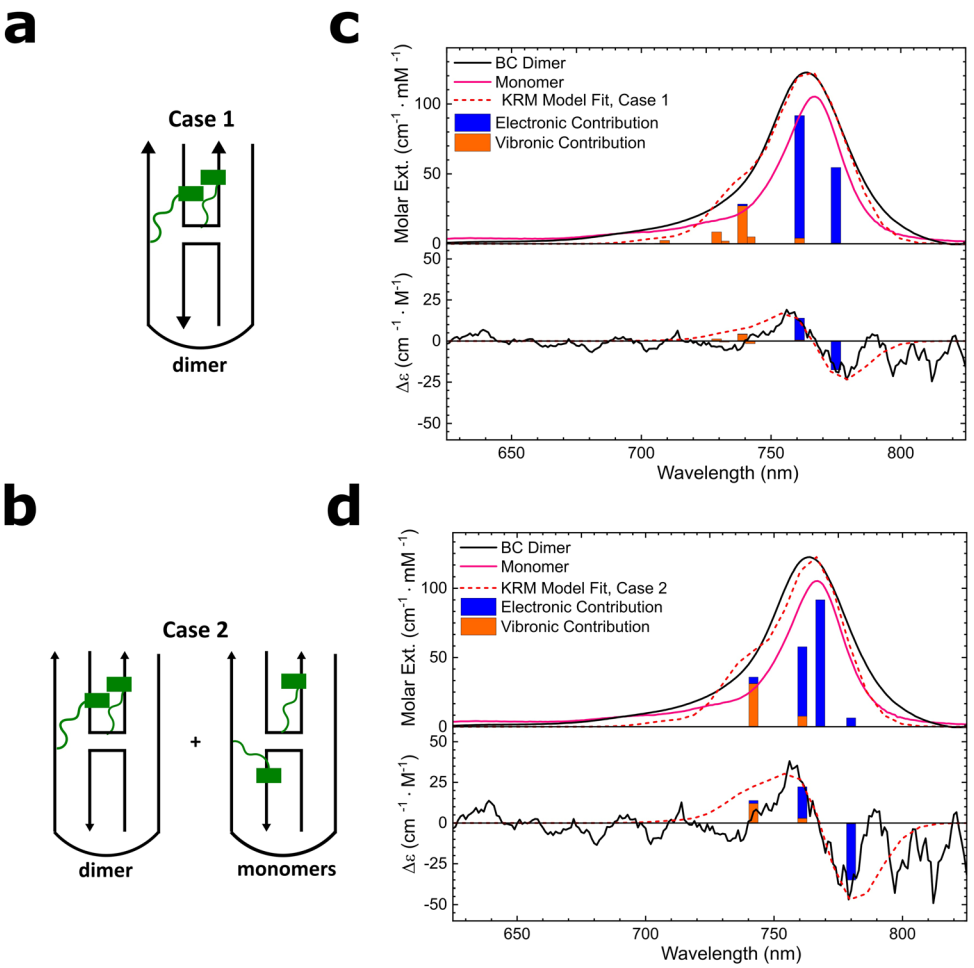

Fig. 6 Two representative cases of bacteriochlorin-HJ system and their KRM modeling. (a) Case 1: a homogeneous system of one dimer population; (b) Case 2: a heterogeneous system of a dimer and monomer populations. (c) and (d) Acquired steady-state absorption and circular dichroism spectra (solid lines) of **BC** monomer and **BC** dimer and theoretical KRM fit (dash line) for (c) Case 1, and (d) Case 2. To account for only 50% of the bacteriochlorin molecules responsible for the observed CD in Case 2, the experimental spectrum magnitude was increased by 2. Vertical bars represent energy eigenstates with heights relative to their transition amplitudes. The bar segments show the relative electronic (blue) *versus* vibronic (orange) contribution to each transition.

Case 2, the "optical" monomers were kept sufficiently distant from the dimer and each other to prevent their coupling. The modeling of Case 2 was performed as 50% dimer and 50% monomer; other dimer–monomer ratios could not be examined due to the limitation of the KRM modeling code.

The theoretical spectra that afforded the best fit for the **BC** dimer systems 1 and 2 are shown in Fig. 6c and d. The J values were 18.5 meV (149 cm^{-1}) and 26.6 meV (214 cm^{-1}), for Cases 1 and 2, respectively. While modeled spectra for both cases exhibited good agreement with the experimental results (Table S5, ESI†), the extracted value of J for Case 2 was in closer agreement with the spectral coupling strength of 27.4 meV from Davydov splitting, and so Case 2 appeared to be a more realistic description of the bacteriochlorin-HJ system. The KRM-derived J of 26.6 meV could be underestimated if the fraction of the intercalated dye population was higher than the modeled 50%.

As a first step to compare the DNA-templated **BC** dimer and the protein-templated **Bchl*a*** dimer, we applied the same spectroscopic modeling approach to calculate J in the natural **Bchl*a*** dimer from the **820B** complex. For this modeling, we used experimental absorption and CD spectra of **820B** reported by Parkes-Loach *et al.* (Fig. S14 and S15, ESI†).[25] Isolated from the LH1 antenna of *Rhodospirillum rubrum*, **820B** consisted of two **Bchl*a*** molecules templated by α/β apoprotein, and lacked the carotenoid and ubiquinone components.[25] Because the absorption of the reference **Bchl*a*** monomer templated by apoprotein was unavailable, we used the reported absorption of "free" **Bchl*a*** (*i.e.*, **777B**) in an aqueous buffer containing methanol from ref. 25 (Fig. S14, ESI†). The absorption maxima of "free" **Bchl*a*** in an aqueous buffer and **820B** dimer were 777 and 820 nm, respectively. The energy difference between "free" **Bchl*a*** and **820B** dimer is likely due to a combination of excitonic coupling and protein-**Bchl*a*** interactions. To account for the protein-**Bchl*a*** interactions in the KRM modeling, we included the offset energy of 50 meV (403 cm^{-1}). Applying a TDM of 7.5 D calculated from the spectrum of **777B**, experimental absorption and CD spectra of **820B** dimer were fitted with the theoretical curves (Fig. 7). The KRM modeling determined J in isolated **820B** dimer to be 35.5 meV (286 cm^{-1}) which was in close agreement with the strength of excitonic coupling of about 300 cm^{-1} calculated by other methods.[78–80] To further characterize the spectral properties of the **BC** and **Bchl*a*** dimers, we compared the origin of excitonic transitions obtained from the computed eigenvalues and eigenvectors vectors of the Holstein-like Hamiltonian.[76] The KRM modeling indicated that the three lowest energy transitions of the **BC** dimer (Case 2) were mostly of electronic origin, *i.e.*, associated with the 0–0 transition. At higher energy (and shorter wavelength), the KRM modeling derived an additional transition of vibronic origin associated with 0–n transition due to weak vibronic coupling. The **Bchl*a*** dimer was characterized by a similar nature of excitonic transitions (Fig. 7). Overall, both **BC** and **Bchl*a*** dimers showed that most of their oscillator strength is of the electronic transitions, which is advantageous in diminishing exciton decoherence originated from the exciton–vibron coupling.[15]

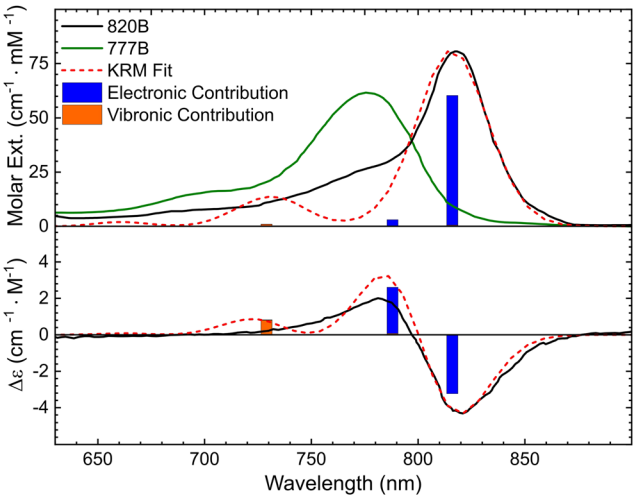

Fig. 7 Steady-state absorption and circular dichroism spectra (solid lines) of **777B** "free" dye in phosphate buffer containing methanol and n-octyl β-D-glucopyranoside, and **820B** dimer templated by apoprotein at 10 μM in phosphate buffer containing n-octyl β-D-glucopyranoside from ref. 25, and theoretical KRM fit (dash line). Vertical bars represent energy eigenstates with heights relative to their transition amplitudes. The bar segments show the relative electronic (blue) *versus* vibronic (orange) contribution to each transition.

As a second step of comparison, we analyzed the geometries of the DNA-templated **BC** dimer (Case 2) and protein-templated **Bchl*a*** dimer. The mutual TDM orientations that afforded the best spectral fit were extracted from the vector spherical and Cartesian coordinates (Fig. 8 and Table S6, ESI†). The dimer geometries were described in terms of center-to-center distance R, and oblique angle α to characterize a deviation from a parallel TDM orientation. In addition, slip angles θ_s were extracted to characterize a displacement of one TDM relative to another and, hence, an aggregate type (*i.e.*, J-dimers exhibit $\theta_s < 54.7^\circ$ while H-dimers exhibit $\theta_s > 54.7^\circ$). In the **Bchl*a*** dimer, TDMs adopted a head-to-tail orientation (J-aggregate) evident in the sharp slip angles of 35° and 7° with a center-to-center distance of 10.1 Å and a 28° obliquity. The TDM orientation in **Bchl*a*** dimer derived by KRM from the spectral data of reconstructed **820B** complex in solution[25] was in close agreement with that of the **Bchl*a*** dimer unit in the crystal structure of LH1-R1 *Thermochromatium tepidum* at a resolution of 1.9 Å.[81] On the other hand, in **BC** dimer, the TDMs adopted a face-to-face orientation (H-aggregate) evident in the slip angles of 97° and 68° with R of 6.7 Å and an oblique angle of 30°. To visualize prospective molecular dimer geometries, the theoretical Q_y polarized along the molecular y-axes were aligned with the extracted TDM vectors; dye macrocycles were oriented arbitrarily face-to-face (Fig. 8).

Discussion

Motivated by reports of exciton delocalization in natural light-harvesting aggregates observed at room temperature,[82–85] we explored the potential to create a similar system using more robust engineering materials: stable and tunable synthetic bacteriochlorin and self-programmable DNA. Namely, by

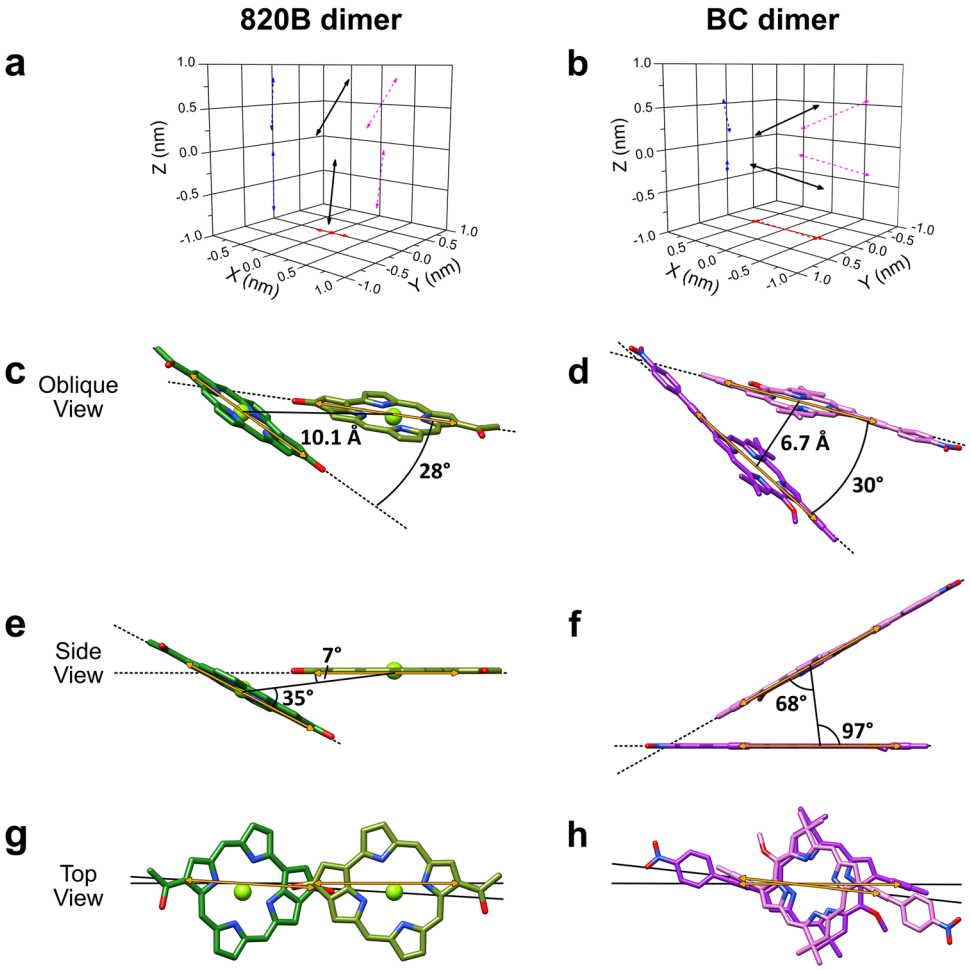

Fig. 8 KRM-derived TMD vector orientations and dimer geometries of isolated **Bchl*a*** dimer (**820B** complex) templated by α/β apoprotein, and **BC** dimer templated by DNA HJ. (a) and (b) Three-dimensional TMD vector plots with TMD plane projections *XY*, *XZ*, and *YZ*. (c)–(h) Dimer geometries with the geometric parameters: center-to-center distance *R* in Å, and oblique angle α in ° shown in the oblique view, and slip angles θ_s in ° shown in the side view. The TDM vectors were aligned with the dye Q_y transitions; the dye core rotations were arbitrarily chosen.

calculating the excitonic hopping parameter *J*, we explored if a DNA-templated dimer of **Bchl*a*** synthetic analog can exhibit exciton delocalization suitable for building excitonic devices. The *J* value represents the strength of dipole–dipole Coulomb coupling, which is the main contribution to the excitonic coupling responsible for exciton delocalization between closely positioned chromophores. In fact, *J* is proportional to the product of TDMs of closely positioned dyes (eqn (S4), ESI†). The magnitude of the TDM primarily stems from the dye core structure but can be enhanced (or reduced) by side substituents and the environment. In natural and synthetic bacteriochlorins, placing auxochromes on opposing pyrrole rings was shown to have the strongest influence on the Q_y TDM, while the addition of the isocyclic ring and central metal had a less pronounced effect.[61] Though synthetic means of installing an isocyclic ring and zinc central metal have been demonstrated,[86,87] we were able to use 3,13-disubstitution alone to achieve a large TDM in the **BC**. Ethynyl-type groups were chosen to enable a robust conjugation with the macrocycle. The resulting synthetic bacteriochlorin **BC** exhibited comparable TDM to natural **Bchl*a***, evident from a comparison of their integrated absorption manifolds (Table 1) and featured a narrower Q_y band with a smaller vibronic progression relative to the natural **Bchl*a***.

Proceeding with covalent templating **BC** *via* DNA, we found that bacteriochlorin was likely in proximity to nucleobases rather than externally bound to DNA based on the Q_y bathochromic shift relative to the "free" dye in ethanol. Further, bacteriochlorin might undergo DNA intercalation based on the weak negative feature in the B_x Soret region of the monomer CD spectrum. We assumed that **BC** was partially intercalated *via* its nitrophenyl substituent so the B_x transition was parallel to the long base pair axis. This assumption was further supported by the molecular geometry of **BC** having bulky geminal dimethyl groups unfavorable for the macrocycle stacking between the base pairs. On the other hand, no hypochromicity nor ICD was observed for the Q_y transition in the monomer spectrum, indicating the electronic interactions between Q_y and DNA bases did not take place, likely due to a large difference in their transition energies. Apparently, the **BC** dimer construct exhibited signatures of the excitonic coupling

and delocalization evident in the small Q_y absorption blueshift and the symmetric bisignate CD couplet. Indeed, a dimer could form between two intercalated dyes. Alternatively, the intercalation could prevent full dye dimerization if several favorable but distant intercalation sites were available on the DNA template. Lacking the direct means to assess the effect of intercalation, we modeled two representative cases: in Case 1, we assumed all dyes covalently attached to DNA were available to form a dimer; in Case 2, 50% of the dyes were sterically unavailable for dimerization, while another 50% of the dyes formed a dimer. The excitonic hopping parameter *J* was calculated to be 18.5 meV and 26.6 meV for Cases 1 and 2, respectively. The *J* values derived for Case 2 agreed with the measured excitonic coupling of 27.4 meV from Davydov splitting.

To directly compare exciton delocalization in *de novo* **BC** dimer templated by DNA and **Bchl*a*** dimer templated by protein, we used the same modeling approach to calculate excitonic hopping parameter *J* in isolated **820B** complex, which consisted of **Bchl*a*** dimer templated by α/β apoprotein.[25] The *J* of **820B**, found to be 35.5 meV (286 cm^{-1}), was in close agreement with the previous calculations by others of the excitonic coupling in the **Bchl*a*** dimer unit of LH1 and LH2 antennas.[79,80,82] While both free **Bchl*a*** and **BC** exhibited comparable TDM magnitudes in the organic solvent, the *J* in DNA-templated *de novo* **BC** dimer was about 10 meV (30%) smaller than that in the **820B** dimer templated by apoprotein in solution. There are several possible explanations for this difference. First, if monomer intercalation occurred, it would disturb efficient dimerization, which would cause an underestimation of *J* in **BC** dimer. Second, the 30% difference between *J* in **Bchl*a*** dimer and **BC** dimer corresponded to the 1.2× difference in the TDM and could be attributed to the medium effects and local polarization of **Bchl*a*** by the protein, which do not occur in DNA. Another difference between the DNA-templated **BC** and protein-templated **Bchl*a*** was found in the dimer geometries. The KRM-derived geometry of **820B** agreed with the geometry of the **Bchl*a*** dimer unit in the LH1 antenna crystal structure at 1.9 Å resolution.[81] The dyes in **820B** were found to be oriented head-to-tail (*i.e.*, a J-aggregate) with a center-to-center distance of 10.1 Å with the 28° oblique angle (Fig. 8). In contrast, the dyes in DNA-templated **BC** dimer adopted an H-aggregate orientation with a center-to-center distance of 6.7 Å and 30° oblique angle. We attributed the difference in the aggregate geometry primarily to the polarity of the medium. In an overall hydrophobic protein environment, the position of each **Bchl*a*** is secured *via* van der Waals interactions with surrounding amino acids, while in an aqueous DNA environment, the orientation of the dyes in the aggregate is governed by minimizing solvent-exposed dye surface as a manifestation of the hydrophobic effect. Therefore, to access oblique or head-to-tail TDM orientations in DNA-templated bacteriochlorin aggregates, future structural designs should be focused on mitigating face-to-face bacteriochlorin alignment utilizing steric substituents or coordination chemistry.

Conclusion

We created a fully synthetic DNA-templated **BC** dimer exhibiting exciton delocalization and featuring stability and functional modularity. Incorporating an NHS linker enabled **BC** covalent attachment to the DNA HJ with spanned arms. A complement of two non-natural side substituents (not present in **Bchl*a***) installed in **BC** afforded spectral properties of **Bchl*a*** and a sufficient TDM to achieve exciton delocalization in the aqueous DNA environment and the absence of pigment–protein interactions. Therefore, the synthetic **BC** enabled us to utilize the unique spectral properties of bacteriochlorins: exceptionally narrow NIR absorption with minimum vibronic contribution, in highly programmable DNA nanotechnology[29] to engineer exciton-based materials. Future structural considerations should be focused on the careful selection of bacteriochlorin substituents and complementary DNA templates guided by systematic studies of bacteriochlorin-DNA non-covalent binding modes. A key goal would be to produce a synthetic bacteriochlorin dimer J-aggregate, in which the TDMs align with head-to-tail orientation. As bacteriochlorin dimers (both natural and synthetic) exhibit excitonic coupling in the weak coupling regime, increasing the number of dyes in the aggregates will be required to achieve high *J*.

Experimental methods

Chemical synthesis

General. ^{1}H and ^{13}C NMR spectra (300, 600 MHz) were collected at room temperature in $CDCl_3$, containing tetramethylsilane as an internal standard. Chemical ^{1}H shifts (δ) were calibrated using $CDCl_3$ residual proton signals at 7.26 ppm. Chemical ^{13}C shifts (δ) were calibrated using $CDCl_3$ residual proton signals at 77.2 ppm. All solvents and commercially available reagents were used as received. Compound **1** was synthesized following the reported procedure.[64]

3,13-Dibromo-5-methoxy-8,8,18,18-tetramethylbacteriochlorin (2)[55]. Following a reported procedure[55] with modifications, a solution of 2,6-di-*tert*-butylpyridine (2.64 mL, 12.2 mmol) in anhydrous dichloromethane (34 mL) in an oven-dried round-bottom flask was stirred for 5 min under argon. Dihydrodipyrrin **1** (200 mg, 0.62 mmol) was added, followed by TMSOTf (0.22 mL, 1.22 mmol) added in two equal portions over 15 min. After stirring the reaction mixture for 1 h at room temperature under argon, one more molar equivalent of TMSOTf (0.11 mL, 0.62 mmol) was added. After stirring for 2 h, **1** was no longer observed by TLC (1 : 1 dichloromethane/hexanes). The reaction mixture was diluted with dichloromethane, washed (saturated aqueous $NaHCO_3$, water, and brine), dried (Na_2SO_4), and concentrated using a rotary evaporator. The crude was purified by column chromatography [silica, dichloromethane/hexanes 1 : 3 then 1 : 1) to afford **2** as a dark green solid (92.0 mg, 92 wt% purity, 54%). ^{1}H NMR ($CDCl_3$, 600 MHz) δ, ppm: −1.98 (brs, 1H), −1.76 (brs, 1H), 1.93 (s, 12H), 4.34 (s, 3H), 4.40 (s, 4H), 8.51 (s, 1H), 8.52 (s, 1H), 8.70, (s, 1H), 8.74 (s, 1H), 8.75 (s, 1H). λ_{abs} (CH_2Cl_2)/nm 349, 370, 504, 723.

3-Bromo-5-methoxy-8,8,18,18-tetramethyl-13-[(4-nitrophenyl)-ethynyl]-bacteriochlorin (3). Following a reported procedure[63] with modifications, a solution of **2** (26.0 mg, 0.054 mmol),

1-ethynyl-4-nitrobenzene (8.2 mg, 0.056 mmol), and anhydrous potassium carbonate (74.2 mg, 0.54 mmol) in *N*,*N*-dimethylformamide (5.4 mL) in an oven-dried 25 mL Schlenk flask was degassed *via* three freeze–pump–thaw cycles. Tetrakis(triphenylphosphine)palladium (24.4 mg, 0.022 mmol) was added, and the reaction mixture was stirred at 80 °C for 16 h under argon. The reaction mixture was diluted with ethyl acetate, washed (water, and brine), dried (Na_2SO_4), and concentrated using a rotary evaporator. The crude was purified by column chromatography (silica, dichloromethane/hexanes 1 : 1 then 3 : 1) to afford **3** as a red solid (8 mg, 28%). ^{1}H NMR ($CDCl_3$, 600 MHz) δ, ppm: −1.94 (brs, 1H), −1.64 (brs, 1H), 1.95 (s, 6H), 1.96 (s, 6H), 4.35 (s, 3H), 4.43 (s, 2H), 4.44 (s, 2H), 8.00 (d, J = 8.7 Hz, 2H), 8.37 (d, J = 8.7 Hz, 2H), 8.51 (s, 1H), 8.62 (s, 1H), 8.75 (d, J = 2.4 Hz, 1H), 8.85 (d, J = 2.0 Hz, 1H), 8.93 (s, 1H); λ_{abs} (CH_2Cl_2)/nm 350, 365, 521, 749. ^{13}C NMR ($CDCl_3$, 600 MHz) δ, ppm: 31.1, 31.2, 45.5, 46.3, 48.1, 51.5, 64.9, 90.8, 94.6, 96.47, 96.51, 98.5, 107.2, 114.2, 124.08, 124.10, 124.9, 125.8, 127.7, 130.9, 132.5, 134.8, 135.4, 135.8, 137.9, 147.2, 156.6, 160.9, 169.6, 171.5. HRMS (ESI/Q-TOF) m/z: [M$^+$] calcd for $C_{33}H_{30}BrN_5O_3$ 623.1532; found 623.1538.

2,5-Dioxopyrrolidin-1-yl hept-6-ynoate (4). Dichloromethane was dried over 3 Å molecular sieves overnight. A solution of 6-heptynoic acid (0.57 g, 4.5 mmol) in dried dichloromethane (20 mL) was treated with *N*-hydroxysuccinimide (0.54 g, 4.73 mmol), and 1-ethyl-3-(3-dimethylaminopropyl)carbodiimide hydrochloride (0.73 g, 4.73 mmol). The reaction mixture was stirred overnight at room temperature. The reaction mixture was extracted with saturated aqueous $NaHCO_3$ (250 mL), washed with water (5 × 50 mL), and brine (3 × 80 mL), dried (Na_2SO_4), and concentrated to afford a white solid (0.73 g, 73%). ^{1}H NMR ($CDCl_3$, 300 MHz) δ, ppm: 1.60–1.70 (m, 2H), 1.84–1.94 (m, 2H), 1.97 (t, J = 2.6 Hz, 1H), 2.25 (td, J_t = 6.9 Hz; J_d = 2.6 Hz; 2H), 2.65 (t, J = 7.4 Hz, 2H), 2.84 (brs, 4H); ^{13}C NMR ($CDCl_3$, 300 MHz) δ, ppm: 18.2, 23.7, 25.8, 27.5, 30.6, 69.2, 83.7, 168.6, 169.3.

5-Methoxy-8,8,18,18-tetramethyl-3-(*N*-hydroxysuccinimidehept-1-ynoate)-13-[(4-nitrophenyl)ethynyl]-bacteriochlorin (BC). A solution of **3** (13.7 mg, 0.022 mmol), **4** (7.1 mg, 0.032 mmol), and triethylamine (1.6 mL) in *N*,*N*-dimethylformamide (3.1 mL) in an oven-dried 25 mL Schlenk flask was degassed *via* three freeze–pump–thaw cycles. Bis(triphenylphosphine)palladium dichloride (1.4 mg, 0.0022 mmol) was added, and the reaction mixture was stirred at 80 °C for 5 h under argon. The reaction mixture was diluted with ethyl acetate (45 mL), washed (water, and brine), dried (Na_2SO_4), and concentrated using a rotary evaporator. The crude was purified by column chromatography (silica, ethyl acetate/hexanes 1 : 1). The product was washed with anhydrous methanol (2 mL) to afford **BC** as a red solid (3 mg, 18%). ^{1}H NMR ($CDCl_3$, 600 MHz) δ, ppm: −1.97 (brs, 1H), −1.60 (brs, 1H), 1.94 (s, 12H), 2.01–2.08 (m, 2H), 2.12–2.27 (m, 2H), 2.82–2.92 (m, 8H), 4.41 (s, 3H), 4.43 (s, 4H), 8.00 (d, J = 8.2 Hz, 2H), 8.37 (d, J = 8.2 Hz, 2H), 8.51 (s, 1H), 8.59 (s, 1H), 8.74 (d, J = 1.9 Hz, 1H), 8.82 (d, J = 1.8 Hz, 1H), 8.90 (s, 1H); ^{13}C NMR ($CDCl_3$, 600 MHz) δ, ppm: 20.2, 24.3, 25.8, 28.3, 30.9, 31.1, 31.2, 45.4, 46.2, 48.3, 51.5, 64.9, 91.1, 94.5, 96.4, 96.8, 98.3, 113.6, 115.2, 124.1, 124.2, 126.7, 131.1, 132.1, 132.5, 134.6, 135.7, 135.8, 137.6, 147.2, 156.9, 160.3, 168.7, 169.3, 171.6. λ_{abs} (toluene)/nm 355, 375, 530, 757. HRMS (ESI/Q-TOF) m/z: [M$^+$] calcd for $C_{44}H_{42}N_6O_7$ 766.3115; found 766.3094.

Bacteriochlorin-DNA templating. DNA oligomers were purchased from IDT (Integrated DNA Technologies, Coralville, IA). Oligomers internally functionalized with amino thymidine sequence modifiers were conjugated with **BC** bacteriochlorin NHS-ester and purified *via* dual high-performance liquid chromatography at IDT. Nonfunctionalized DNA oligomers were purified by standard desalting at IDT. All DNA oligomers were rehydrated in ultrapure water (Barnstead Nanopure, Thermo Scientific) to prepare 35–40 μM stock solutions. The stock concentrations of single DNA strands were verified spectroscopically on a NanoDrop One Microvolume UV-Vis Spectrophotometer (Thermo Scientific). The DNA HJ theoretical extinction coefficient ε_{260} was calculated to be 956 500 M^{-1} cm^{-1}. The bacteriochlorin-HJ samples were prepared by combining equimolar amounts of three oligomers in 1× TBE, 15 mM $MgCl_2$ pH 8 buffer solution to the final DNA concentrations of 1.5 μM and 4.0 μM for steady-state absorption and CD measurements, respectively. All DNA samples were allowed to hybridize by incubation for 2 h at room temperature.

Optical characterization

UV-vis spectra were recorded in duplicates at room temperature on a single-beam Cary 5000 UV-vis-NIR spectrophotometer (Agilent Technologies) in a quartz cuvette with a 1 cm path length (Starna). Absorption spectra were monitored over a 230–900 nm wavelength range. CD measurements were performed on a JACSO-J1500 spectropolarimeter in a 1 cm path-length quartz cuvette (Jasco). Spectra were recorded over the 230–900 nm wavelength range at a speed of 200 nm min^{-1}, 2 s data integration time, 1 nm bandwidth, and 9 accumulations.

Author contributions

Conceptualization, OAM; methodology, OAM, BY, WBK; validation, OAM, DRW, LKP; formal analysis, OAM, DRW, LKP; investigation, OAM, DRW, LKP; data curation, OAM, BY, WBK; writing—original draft preparation, OAM, DRW; writing—review and editing, DBT, OAM, BY, RDP, WBK, LKP, JL, DRW; visualization, OAM, DRW, LKP; supervision, OAM, JL, WBK; funding acquisition, OAM, RDP, BY, JL, WBK. All authors have read and agreed to the published version of the manuscript.

Conflicts of interest

The authors declare no competing financial interests.

Acknowledgements

This research was supported wholly by the U.S. Department of Energy (DOE), Office of Basic Energy Sciences, Materials Sciences and Engineering Division and DOE's Established Program to Stimulate Competitive Research (EPSCoR) program under Award No. DE-SC0020089. The ESI/Q-TOF of

bacteriochlorin molecules were obtained at the Biomolecular Research Center at Boise State, which is supported in part by the Institutional Development Awards (IDeA) from the National Institute of General Medical Sciences (Award no. P20GM103408) and the National Institutes of Health (Award no. P20GM109095), the National Science Foundation (Award no. 0619793 and 0923535), the MJ Murdock Charitable Trust, and the Idaho State Board of Education. We thank Dr Shibani Basu for the assistance with recording a circular dichroism spectrum of **BC** dimer HJ construct. We thank Dr Natalya Hallstrom for the assistance with PAGE electrophoresis of bacteriochlorin-DNA constructs.

References

1 R. J. Cogdell, N. W. Isaacs, T. D. Howard, K. McLuskey, N. J. Fraser and S. M. Prince, How Photosynthetic Bacteria Harvest Solar Energy, *J. Bacteriol.*, 1999, **181**, 3869–3879.

2 X. Hu, A. Damjanovic, T. Ritz and K. Schulten, Architecture and mechanism of the light-harvesting apparatus of purple bacteria, *Proc. Natl. Acad. Sci. U. S. A.*, 1998, **95**, 5935–5941.

3 M. Kasha, Energy Transfer Mechanisms and the Molecular Exciton Model for Molecular Aggregates, *Radiat. Res.*, 1963, **20**, 55–70.

4 M. Chachisvilis, O. Kuhn, T. Pullerits and V. Sundstrom, Excitons in photosynthetic purple bacteria: Wavelike motion or incoherent hopping?, *J. Phys. Chem. B*, 1997, **101**, 7275–7283.

5 T. Mirkovic, E. E. Ostroumov, J. M. Anna, R. Van Grondelle, Govindjee and G. D. Scholes, Light Absorption and Energy Transfer in the Antenna Complexes of Photosynthetic Organisms, *Chem. Rev.*, 2017, **117**, 249–293.

6 M. Dahlbom, T. Pullerits, S. Mukamel and V. Sundström, Exciton Delocalization in the B850 Light-Harvesting Complex: Comparison of Different Measures, *J. Phys. Chem. B*, 2001, **105**, 5515–5524.

7 G. D. Scholes and G. Rumbles, Excitons in nanoscale systems, *Nat. Mater.*, 2006, **5**, 683–696.

8 G. D. Scholes, G. R. Fleming, A. Olaya-Castro and R. van Grondelle, Lessons from nature about solar light harvesting, *Nat. Chem.*, 2011, **3**, 763–774.

9 G. D. Scholes, Quantum Biology Coherence in photosynthesis, *Nat. Phys.*, 2011, **7**, 448–449.

10 M. R. Wasielewski, Self-Assembly Strategies for Integrating Light Harvesting and Charge Separation in Artificial Photosynthetic Systems, *Acc. Chem. Res.*, 2009, **42**, 1910–1921.

11 F. Garo and R. Haner, A DNA-based light-harvesting antenna, *Angew. Chem., Int. Ed.*, 2012, **51**, 916–919.

12 X. Wang, R. Sha, W. B. Knowlton, N. C. Seeman, J. W. Canary and B. Yurke, Exciton Delocalization in a DNA-Templated Organic Semiconductor Dimer Assembly, *ACS Nano*, 2022, **16**, 1301–1307.

13 D. L. Kellis, S. M. Rehn, B. L. Cannon, P. H. Davis, E. Graugnard, J. Lee, B. Yurke and W. B. Knowlton, DNA-mediated excitonic upconversion FRET switching, *New J. Phys.*, 2015, **17**, 115007.

14 D. L. Kellis, C. Sarter, B. L. Cannon, P. H. Davis, E. Graugnard, J. Lee, R. D. Pensack, T. Kolmar, A. Jäschke, B. Yurke and W. B. Knowlton, An All-Optical Excitonic Switch Operated in the Liquid and Solid Phases, *ACS Nano*, 2019, **13**, 2986–2994.

15 B. Yurke, R. Elliott and A. Sup, Implementation of a Frenkel exciton-based controlled phase shifter, *Phys. Rev. A*, 2023, **107**, 012603.

16 M. R. Wasielewski, M. D. E. Forbes, N. L. Frank, K. Kowalski, G. D. Scholes, J. Yuen-Zhou, M. A. Baldo, D. E. Freedman, R. H. Goldsmith, T. Goodson, M. L. Kirk, J. K. McCusker, J. P. Ogilvie, D. A. Shultz, S. Stoll and K. B. Whaley, Exploiting chemistry and molecular systems for quantum information science, *Nat. Rev. Chem.*, 2020, **4**, 490–504.

17 B. Yurke, in *Visions of DNA nanotechnology at 40 for the next 40 – a tribute to Nadrian C. Seeman*, ed. N. Jonoska and E. Winfree, Springer, Singapore, 2023, pp. 125–169.

18 M. A. Castellanos, A. Dodin and A. P. Willard, On the design of molecular excitonic circuits for quantum computing: The universal quantum gates, *Phys. Chem. Chem. Phys.*, 2020, **22**, 3048–3057.

19 G. S. Beddard and G. Porter, Concentration quenching in chlorophyll, *Nature*, 1976, **260**, 366–367.

20 R. J. Cogdell, T. D. Howard, N. W. Isaacs, K. McLuskey and A. T. Gardiner, Structural factors which control the position of the Qy absorption band of bacteriochlorophyll a in purple bacterial antenna complexes, *Photosynth. Res.*, 2002, **74**, 135–141.

21 E. Wientjes, G. Roest and R. Croce, From red to blue to far-red in Lhca4: How does the protein modulate the spectral properties of the pigments?, *Biochim. Biophys. Acta, Bioenerg.*, 2012, **1817**, 711–717.

22 K. Sauer, J. R. L. Smith and A. J. Schultz, The Dimerization of Chlorophyll a, Chlorophyll b, and Bacteriochlorophyll in Solution1, *J. Am. Chem. Soc.*, 1966, **88**, 2681–2688.

23 J. Linnanto, J. A. I. Oksanen and J. E. I. Korppi-Tommola, Exciton interactions in self-organised bacteriochlorophyll a – aggregates, *Phys. Chem. Chem. Phys.*, 2002, **4**, 3061–3070.

24 M. R. Wasielewski, U. H. Smith, B. T. Cope and J. J. Katz, A synthetic biomimetic model of special pair bacteriochlorophyll a, *J. Am. Chem. Soc.*, 1977, **99**, 4173.

25 P. S. Parkes-Loach, J. R. Sprinkle and P. A. Loach, Reconstitution of the B873 light-harvesting complex of Rhodospirillum rubrum from the separately isolated. alpha.- and .beta. -polypeptides and bacteriochlorophyll a, *Biochemistry*, 1988, **27**, 2718–2727.

26 I. Cohen-Ofri, M. van Gastel, J. Grzyb, A. Brandis, I. Pinkas, W. Lubitz and D. Noy, Zinc-Bacteriochlorophyllide Dimers in de Novo Designed Four-Helix Bundle Proteins. A Model System for Natural Light Energy Harvesting and Dissipation, *J. Am. Chem. Soc.*, 2011, **133**, 9526–9535.

27 K. R. Reddy, J. Jiang, M. Krayer, M. A. Harris, J. W. Springer, E. Yang, J. Jiao, D. M. Niedzwiedzki, D. Pandithavidana, P. S. Parkes-Loach, C. Kirmaier, P. A. Loach, D. F. Bocian, D. Holten and J. S. Lindsey, Palette of lipophilic

bioconjugatable bacteriochlorins for construction of biohybrid light-harvesting architectures, *Chem. Sci.*, 2013, **4**, 2036–2053.

28 N. C. Seeman, Structural DNA nanotechnology: an overview, *Methods Mol. Biol.*, 2005, **303**, 143–166.

29 N. C. Seeman, DNA in a material world, *Nature*, 2003, **421**, 427–431.

30 V. L. Malinovskii, D. Wenger and R. Haner, Nucleic acid-guided assembly of aromatic chromophores, *Chem. Soc. Rev.*, 2010, **39**, 410–422.

31 H. Kashida, H. Asanuma and M. Komiyama, Alternating hetero H aggregation of different dyes by interstrand stacking from two DNA-dye conjugates, *Angew. Chem., Int. Ed.*, 2004, **43**, 6522–6525.

32 H. Kashida, M. Tanaka, S. Baba, T. Sakamoto, G. Kawai, H. Asanuma and M. Komiyama, Covalent incorporation of methyl red dyes into double-stranded DNA for their ordered clustering, *Chem. - Eur. J.*, 2006, **12**, 777–784.

33 T. Fujii, H. Kashida and H. Asanuma, Analysis of Coherent Heteroclustering of Different Dyes by Use of Threoninol Nucleotides for Comparison with the Molecular Exciton Theory, *Chem. – Eur. J.*, 2009, **15**, 10092–10102.

34 J. Dietzsch, D. Bialas, J. Bandorf, F. Würthner and C. Höbartner, Tuning Exciton Coupling of Merocyanine Nucleoside Dimers by RNA, DNA and GNA Double Helix Conformations, *Angew. Chem., Int. Ed.*, 2022, **61**, e202116783.

35 B. L. Cannon, D. L. Kellis, L. K. Patten, P. H. Davis, J. Lee, E. Graugnard, B. Yurke and W. B. Knowlton, Coherent Exciton Delocalization in a Two-State DNA-Templated Dye Aggregate System, *J. Phys. Chem. A*, 2017, **121**, 6905–6916.

36 B. L. Cannon, L. K. Patten, D. L. Kellis, P. H. Davis, J. Lee, E. Graugnard, B. Yurke and W. B. Knowlton, Large Davydov Splitting and Strong Fluorescence Suppression: An Investigation of Exciton Delocalization in DNA-Templated Holliday Junction Dye Aggregates, *J. Phys. Chem. A*, 2018, **122**, 2086–2095.

37 P. D. Cunningham, Y. C. Kim, S. A. Diaz, S. Buckhout-White, D. Mathur, I. L. Medintz and J. S. Melinger, Optical Properties of Vibronically Coupled Cy3 Dimers on DNA Scaffolds, *J. Phys. Chem. B*, 2018, **122**, 5020–5029.

38 S. M. Hart, W. J. Chen, J. L. Banal, W. P. Bricker, A. Dodin, L. Markova, Y. Vyborna, A. P. Willard, R. Häner, M. Bathe and G. S. Schlau-Cohen, Engineering couplings for exciton transport using synthetic DNA scaffolds, *Chem*, 2021, **7**, 752–773.

39 D. Heussman, J. Kittell, L. Kringle, A. Tamimi, P. H. von Hippel and A. H. Marcus, Measuring local conformations and conformational disorder of (Cy3)(2) dimer labeled DNA fork junctions using absorbance, circular dichroism and two-dimensional fluorescence spectroscopy, *Faraday Discuss.*, 2019, **216**, 211–235.

40 R. J. Mazuski, S. A. Díaz, R. E. Wood, L. T. Lloyd, W. P. Klein, D. Mathur, J. S. Melinger, G. S. Engel and I. L. Medintz, Ultrafast Excitation Transfer in Cy5 DNA Photonic Wires Displays Dye Conjugation and Excitation Energy Dependency, *J. Phys. Chem. Lett.*, 2020, 4163–4172, DOI: 10.1021/acs.jpclett.0c01020,.

41 F. Nicoli, M. K. Roos, E. A. Hemmig, M. Di Antonio, R. de Vivie-Riedle and T. Liedl, Proximity-Induced H-Aggregation of Cyanine Dyes on DNA-Duplexes, *J. Phys. Chem. A*, 2016, **120**, 9941–9947.

42 S. K. Roy, O. A. Mass, D. L. Kellis, C. K. Wilson, J. A. Hall, B. Yurke and W. B. Knowlton, Exciton Delocalization and Scaffold Stability in Bridged Nucleotide-Substituted, DNA Duplex-Templated Cyanine Aggregates, *J. Phys. Chem. B*, 2021, **125**, 13670–13684.

43 K. M. Duncan, H. M. Byers, M. E. Houdek, S. K. Roy, A. Biaggne, M. S. Barclay, L. K. Patten, J. S. Huff, D. L. Kellis, C. K. Wilson, J. Lee, P. H. Davis, O. A. Mass, L. Li, D. B. Turner, J. A. Hall, W. B. Knowlton, B. Yurke and R. D. Pensack, Electronic Structure and Excited-State Dynamics of DNA-Templated Monomers and Aggregates of Asymmetric Polymethine Dyes, *J. Phys. Chem. A*, 2023, **127**, 4901–4918.

44 M. S. Barclay, S. K. Roy, J. S. Huff, O. A. Mass, D. B. Turner, C. K. Wilson, D. L. Kellis, E. A. Terpetschnig, J. Lee, P. H. Davis, B. Yurke, W. B. Knowlton and R. D. Pensack, Rotaxane rings promote oblique packing and extended lifetimes in DNA-templated molecular dye aggregates, *Commun. Chem.*, 2021, **4**, 19.

45 M. S. Barclay, C. K. Wilson, S. K. Roy, O. A. Mass, O. M. Obukhova, R. P. Svoiakov, A. L. Tatarets, A. U. Chowdhury, J. S. Huff, D. B. Turner, P. H. Davis, E. A. Terpetschnig, B. Yurke, W. B. Knowlton, J. Lee and R. D. Pensack, Oblique Packing and Tunable Excitonic Coupling in DNA-Templated Squaraine Rotaxane Dimer Aggregates, *ChemPhotoChem*, 2022, **6**, e202200039.

46 S. Basu, K. Cervantes-Salguero, B. Yurke, W. B. Knowlton, J. Lee and O. A. Mass, Photocrosslinking Probes Proximity of Thymine Modifiers Tethering Excitonically Coupled Dye Aggregates to DNA Holliday Junction, *Molecules*, 2022, **27**, 4006.

47 O. A. Mass, C. K. Wilson, G. Barcenas, E. A. Terpetschnig, O. M. Obukhova, O. S. Kolosova, A. L. Tatarets, L. Li, B. Yurke, W. B. Knowlton, R. D. Pensack and J. Lee, Influence of Hydrophobicity on Excitonic Coupling in DNA-Templated Indolenine Squaraine Dye Aggregates, *J. Phys. Chem. C*, 2022, **126**, 3475–3488.

48 O. A. Mass, C. K. Wilson, S. K. Roy, M. S. Barclay, L. K. Patten, E. A. Terpetschnig, J. Lee, R. D. Pensack, B. Yurke and W. B. Knowlton, Exciton Delocalization in Indolenine Squaraine Aggregates Templated by DNA Holliday Junction Scaffolds, *J. Phys. Chem. B*, 2020, **124**, 9636–9647.

49 K. M. Duncan, D. L. Kellis, J. S. Huff, M. S. Barclay, J. Lee, D. B. Turner, P. H. Davis, B. Yurke, W. B. Knowlton and R. D. Pensack, Symmetry Breaking Charge Transfer in DNA-Templated Perylene Dimer Aggregates, *Molecules*, 2022, **27**, 6612.

50 A. Brewer, G. Siligardi, C. Neylon and E. Stulz, Introducing structural flexibility into porphyrin–DNA zipper arrays, *Org. Biomol. Chem.*, 2011, **9**, 777–782.

51 D. G. Singleton, R. Hussain, G. Siligardi, P. Kumar, P. J. Hrdlicka, N. Berova and E. Stulz, Increased duplex stabilization

in porphyrin-LNA zipper arrays with structure dependent exciton coupling, *Org. Biomol. Chem.*, 2016, **14**, 149–157.
52 M. Vybornyi, A. L. Nussbaumer, S. M. Langenegger and R. Häner, Assembling Multiporphyrin Stacks Inside the DNA Double Helix, *Bioconjugate Chem.*, 2014, **25**, 1785–1793.
53 M. Endo, M. Fujitsuka and T. Majima, Diastereochemically Controlled Porphyrin Dimer Formation on a DNA Duplex Scaffold, *J. Org. Chem.*, 2008, **73**, 1106–1112.
54 B. Albinsson, J. K. Hannestad and K. Börjesson, Functionalized DNA nanostructures for light harvesting and charge separation, *Coord. Chem. Rev.*, 2012, **256**, 2399–2413.
55 M. Krayer, M. Ptaszek, H.-J. Kim, K. R. Meneely, D. Fan, K. Secor and J. S. Lindsey, Expanded Scope of Synthetic Bacteriochlorins *via* Improved Acid Catalysis Conditions and Diverse Dihydrodipyrrin-Acetals, *J. Org. Chem.*, 2010, **75**, 1016–1039.
56 H.-J. Kim and J. S. Lindsey, De Novo Synthesis of Stable Tetrahydroporphyrinic Macrocycles: Bacteriochlorins and a Tetradehydrocorrin, *J. Org. Chem.*, 2005, **70**, 5475–5486.
57 O. Kühn, T. Renger and V. May, Theory of exciton-vibrational dynamics in molecular dimers, *Chem. Phys.*, 1996, **204**, 99–114.
58 M. Taniguchi, D. L. Cramer, A. D. Bhise, H. L. Kee, D. F. Bocian, D. Holten and J. S. Lindsey, Accessing the near-infrared spectral region with stable, synthetic, wavelength-tunable bacteriochlorins, *New J. Chem.*, 2008, **32**, 947–958.
59 H. Jing, S. Liu, J. Jiang, V.-P. Tran, J. Rong, P. Wang and J. S. Lindsey, Meso bromination and derivatization of synthetic bacteriochlorins, *New J. Chem.*, 2022, **46**, 5556–5572.
60 D. Abramavicius, B. Palmieri, D. V. Voronine, F. Šanda and S. Mukamel, Coherent Multidimensional Optical Spectroscopy of Excitons in Molecular Aggregates; Quasiparticle versus Supermolecule Perspectives, *Chem. Rev.*, 2009, **109**, 2350–2408.
61 E. Yang, C. Kirmaier, M. Krayer, M. Taniguchi, H.-J. Kim, J. R. Diers, D. F. Bocian, J. S. Lindsey and D. Holten, Photophysical Properties and Electronic Structure of Stable, Tunable Synthetic Bacteriochlorins: Extending the Features of Native Photosynthetic Pigments, *J. Phys. Chem. B*, 2011, **115**, 10801–10816.
62 O. Mass, M. Taniguchi, M. Ptaszek, J. W. Springer, K. M. Faries, J. R. Diers, D. F. Bocian, D. Holten and J. S. Lindsey, Structural characteristics that make chlorophylls green: interplay of hydrocarbon skeleton and substituents, *New J. Chem.*, 2011, **35**, 76–88.
63 Z. Q. Yu and M. Ptaszek, Multifunctional Bacteriochlorins from Selective Palladium-Coupling Reactions, *Org. Lett.*, 2012, **14**, 3708–3711.
64 M. Krayer, T. Balasubramanian, C. Ruzie, M. Ptaszek, D. L. Cramer, M. Taniguchi and J. S. Lindsey, Refined syntheses of hydrodipyrrin precursors to chlorin and bacteriochlorin building blocks, *J. Porphyrins phthalocyanines*, 2009, **13**, 1098–1110.
65 C. Hyeon, J. Lee, J. Yoon, S. Hohng and D. Thirumalai, Hidden complexity in the isomerization dynamics of Holliday junctions, *Nat. Chem.*, 2012, **4**, 907–914.
66 O. A. Mass, S. Basu, L. K. Patten, E. A. Terpetschnig, A. I. Krivoshey, A. L. Tatarets, R. D. Pensack, B. Yurke, W. B. Knowlton and J. Lee, Exciton Chirality Inversion in Dye Dimers Templated by DNA Holliday Junction, *J. Phys. Chem. Lett.*, 2022, **13**, 10688–10696.
67 A. Kimball, Q. Guo, M. Lu, R. P. Cunningham, N. R. Kallenbach, N. C. Seeman and T. D. Tullius, Construction and analysis of parallel and antiparallel Holliday junctions, *J. Biol. Chem.*, 1990, **265**, 6544–6547.
68 L. K. Arciszewska, I. Grainge and D. J. Sherratt, Action of site-specific recombinases XerC and XerD on tethered Holliday junctions, *EMBO J.*, 1997, **16**, 3731–3743.
69 PhotochemCAD, **https://www.photochemcad.com/**, (accessed January 18, 2023).
70 N. N. Esemoto, Z. Yu, L. Wiratan, A. Satraitis and M. Ptaszek, Bacteriochlorin Dyads as Solvent Polarity Dependent Near-Infrared Fluorophores and Reactive Oxygen Species Photosensitizers, *Org. Lett.*, 2016, **18**, 4590–4593.
71 N. C. Garbett, P. A. Ragazzon and J. B. Chaires, Circular dichroism to determine binding mode and affinity of ligand–DNA interactions, *Nat. Protoc.*, 2007, **2**, 3166–3172.
72 M. H. Nasir, E. Jabeen, R. Qureshi, F. L. Ansari, A. Shaukat, U. Nasir and A. Ahmed, Investigation of redox mechanism and DNA binding of novel 2-(x-nitrophenyl)-5-nitrobenzimidazole (x = 2, 3 and 4), *Biophys. Chem.*, 2020, **258**, 106316.
73 C. A. M. Seidel, A. Schulz and M. H. M. Sauer, Nucleobase-Specific Quenching of Fluorescent Dyes. 1. Nucleobase One-Electron Redox Potentials and Their Correlation with Static and Dynamic Quenching Efficiencies, *J. Phys. Chem.*, 1996, **100**, 5541–5553.
74 H. Asanuma, T. Fujii, T. Kato and H. Kashida, Coherent interactions of dyes assembled on DNA, *J. Photochem. Photobiol., C*, 2012, **13**, 124–135.
75 J. S. Huff, P. H. Davis, A. Christy, D. L. Kellis, N. Kandadai, Z. S. D. Toa, G. D. Scholes, B. Yurke, W. B. Knowlton and R. D. Pensack, DNA-Templated Aggregates of Strongly Coupled Cyanine Dyes: Nonradiative Decay Governs Exciton Lifetimes, *J. Phys. Chem. Lett.*, 2019, **10**, 2386–2392.
76 T. Holstein, Studies of polaron motion: Part I. The molecular-crystal model, *Ann. Phys.*, 1959, **8**, 325–342.
77 V. Czikklely, H. D. Forsterling and H. Kuhn, Extended dipole model for aggregates of dye molecules, *Chem. Phys. Lett.*, 1970, **6**, 207–210.
78 K. Sauer, R. J. Cogdell, S. M. Prince, A. Freer, N. W. Isaacs and H. Scheer, Structure-Based Calculations of the Optical Spectra of the LH2 Bacteriochlorophyll-Protein Complex from Rhodopseudomonas acidophila, *Photochem. Photobiol.*, 1996, **64**, 564–576.
79 G. D. Scholes, I. R. Gould, R. J. Cogdell and G. R. Fleming, Ab Initio Molecular Orbital Calculations of Electronic Couplings in the LH2 Bacterial Light-Harvesting Complex of Rps. Acidophila, *J. Phys. Chem. B*, 1999, **103**, 2543–2553.
80 S. Tretiak, C. Middleton, V. Chernyak and S. Mukamel, Bacteriochlorophyll and Carotenoid Excitonic Couplings in the LH2 System of Purple Bacteria, *J. Phys. Chem. B*, 2000, **104**, 9540–9553.
81 L.-J. Yu, M. Suga, Z.-Y. Wang-Otomo and J.-R. Shen, Structure of photosynthetic LH1–RC supercomplex at 1.9 Å resolution, *Nature*, 2018, **556**, 209–213.

82 D. C. Arnett, C. C. Moser, P. L. Dutton and N. F. Scherer, The First Events in Photosynthesis: Electronic Coupling and Energy Transfer Dynamics in the Photosynthetic Reaction Center from Rhodobacter sphaeroides, *J. Phys. Chem. B*, 1999, **103**, 2014–2032.

83 R. Kumble, S. Palese, R. W. Visschers, P. Leslie Dutton and R. M. Hochstrasser, Ultrafast dynamics within the B820 subunit from the core (LH-1) antenna complex of Rs. rubrum, *Chem. Phys. Lett.*, 1996, **261**, 396–404.

84 T. Brixner, J. Stenger, H. M. Vaswani, M. Cho, R. E. Blankenship and G. R. Fleming, Two-dimensional spectroscopy of electronic couplings in photosynthesis, *Nature*, 2005, **434**, 625–628.

85 D. B. Turner, K. E. Wilk, P. M. G. Curmi and G. D. Scholes, Comparison of Electronic and Vibrational Coherence Measured by Two-Dimensional Electronic Spectroscopy, *J. Phys. Chem. Lett.*, 2011, **2**, 1904–1911.

86 M. Krayer, E. Yang, J. R. Diers, D. F. Bocian, D. Holten and J. S. Lindsey, De novo synthesis and photophysical characterization of annulated bacteriochlorins. Mimicking and extending the properties of bacteriochlorophylls, *New J. Chem.*, 2011, **35**, 587–601.

87 C.-Y. Chen, E. Sun, D. Fan, M. Taniguchi, B. E. McDowell, E. Yang, J. R. Diers, D. F. Bocian, D. Holten and J. S. Lindsey, Synthesis and Physicochemical Properties of Metallobacteriochlorins, *Inorg. Chem.*, 2012, **51**, 9443–9464.